

**SYNTHESIS AND CHARACTERIZATION OF CARBON COATED AND  
NITROGEN DOPED TiO<sub>2</sub> FOR ENHANCED PHOTOCATALYTIC  
DEGRADATION OF ORGANIC POLLUTANTS UNDER UV-VIS AND  
VISIBLE LIGHT IRRADIATION**

by

**WAN IZHAN NAWAWI WAN ISMAIL**

**Thesis submitted in fulfillment of the requirements for the degree of Doctor of  
Philosophy**

**2013**

i

## ACKNOWLEDGEMENTS

IN THE NAME OF ALLAH, THE MOST GRACIOUS AND MOST MERCIFUL

Thanks to Allah S.W.T for giving me the opportunity to do and complete this thesis successfully. A journey is easier when you travel together. Interdependence is certainly more valuable than independence. This thesis is the results of five years of works whereby I have been accompanied and supported by many people. It is a pleasant aspect that I have now opportunity to express my gratitude to all of them.

The first person I would like to thank is my supervisor; Prof. Mohd Asri Mohd Nawi whose help, stimulating suggestions and encouragement helped me in all the time of research and writing of this thesis, also kept an eye on the progress of my work and always available when I needed his advises. I would also like to extend my thanks to Institut Pengajian Siswazah, Universiti Sains Malaysia and for research funds (Science fund Grant: 305/PKIMIA/613402 and FRGS Grant: 203/PKIMIA/ 6711228) from Ministry of Science Technology & Innovation (MOSTI), Malaysia. Special thanks to all my members for their kindness and generous assistant throughout this research and also those had contributed either directly or indirectly to this research. Their co-operations are not easily forgotten.

Finally, I would like to express my special gratitude to my dearest family especially lovely parents; Wan Ismail and Jawahir Daud. For my wife: Nadina Anuar. My Parent in Law; Anuar Ahmad and Zaharah Ramli for their love, understanding, never ending encouragement and financial support to preceed and complete my research studies in Universiti Sains Malaysia.

## TABLE OF CONTENTS

	Page
Acknowledgments	ii
Table of Contents	iii
List of Tables	x
List of Figures	xii
List of Abbreviations	xviii
Abstrak	xix
Abstract	xxi
 CHAPTER ONE - INTRODUCTION	
1.1 Environmental Problems	1
1.2 Advance Oxidation Process (AOP)	1
1.3 Heterogeneous Photocatalysis	4
1.4 Principles of semiconductor photocatalysis	8
1.5 TiO <sub>2</sub> as photocatalyst	13
1.6	18
1.7 Improving TiO <sub>2</sub> photocatalytic activity	22
1.7.1 Modification with metal	23
1.7.2 Modification with nonmetals	24
1.7.2.1 Nitrogen doped TiO <sub>2</sub>	24
1.7.2.2 Sulphur doped TiO <sub>2</sub>	26
1.7.2.3 TiO <sub>2</sub> -Carbon combination	27
1.7.3 Modification with CdS (composite semiconductor)	29
1.7.4 Modification with surface sensitizer	31

1.8	Potential of the natural polymers for TiO <sub>2</sub> sensitizer	32
1.8.1	Epoxidized Natural Rubber (ENR)	32
1.8.2	Peat Coagulant	35
1.8.3	Urea	37
1.9	Organic pollutants	38
1.9.1	Anionic Reactive Red 4 dye (RR4)	39
1.9.2	Cationic Methylene Blue dye	40
1.9.3	Phenol	41
1.10	Problem statements	42
1.11	Research objectives	43
<b>CHAPTER TWO - MATERIALS AND METHODS</b>		
2.1	Reagents and chemicals.	45
2.2	Photoreactor and light sources	46
2.3	Instruments and equipments	48
2.4	Preparation of standard solutions	49
2.4.1	Preparation of RR4 dye standard solution	49
2.4.2	Preparation of MB standard solution	49
2.4.3	Preparation of phenol standard solution	50
2.4.4	Preparation of COD reagent for mineralization study of model pollutants.	50
2.5	Modification of TiO <sub>2</sub>	51
2.5.1	Preparation of the carbon/ nitrogen precursors	51
2.5.2	Preparation of the carbon coated TiO <sub>2</sub> (Sigma) photocatalyst (C coated TiO <sub>2</sub> )	52
2.5.3	Preparation of the carbon coated TiO <sub>2</sub> -P25 photocatalyst using peat coagulant as the precursor (C coated TiO <sub>2</sub> -P25)	53

2.5.4	Preparation of the carbon coated nitrogen doped TiO <sub>2</sub> -P25 photocatalyst using urea as the precursor (C coated N doped TiO <sub>2</sub> -P25)	54
2.6	Optimization Studies on the Preparation of C coated TiO <sub>2</sub>	56
2.6.1	Effect of different amount of precursors on the photocatalytic efficiency of the modified photocatalyst	56
2.6.1.1	Effect of different amount of ENR	56
2.6.1.2	Effect of different amount of peat	57
2.6.1.3	Effect of different amount of urea	57
2.6.2	Effect of temperature on the photocatalytic efficiency of the modified photocatalyst	57
2.6.3.1	Effect of calcination temperature towards photocatalytic efficiency of ENR-TiO <sub>2</sub>	58
2.6.3.2	Effect of calcination temperature towards photocatalytic efficiency of peat-(TiO <sub>2</sub> -P25)	58
2.6.3.3	Effect of temperature towards photocatalytic efficiency of urea-(TiO <sub>2</sub> -P25)	59
2.7	Characterization of the photocatalyst systems	59
2.7.1	SEM analysis	59
2.7.2	CHNS analysis	59
2.7.3	UV-Vis diffused reflectance	60
2.7.4	BET surface area analysis	60
2.7.5	X-ray diffraction (XRD) analysis	60
2.7.6	Photoluminescent analysis	61
2.7.7	HRTEM analysis	61
2.7.8	XPS analysis	62
2.8	Photocatalytic degradation of RR4, MB and phenol	62
2.9	Determination of the rate constants for the photocatalytic degradation of model pollutants	63

2.10	Adsorption study	64
2.11	The effect of operational parameters on the photocatalytic efficiency of modified photocatalyst in the degradation of RR4 dye	65
	2.11.1 Effect of initial dye concentration on the photocatalytic efficiency of the modified photocatalyst	65
	2.11.2 Effect of the photocatalyst loading	65
	2.11.3 Effect of the aeration flow rate	66
	2.11.4 Effect of initial pH values of the RR4 dye solutions	66
2.12	Determination of point of the zero charge ( $\text{pH}_{\text{zpc}}$ ) for the unmodified and modified photocatalyst	67
2.13	Mineralization study	67
	2.13.1 Preparation of COD reagent of chemical oxygen demand (COD) reagent	69
	2.13.2 Chemical oxygen demand (COD)	68
	2.13.3 Total organic carbon (TOC)	69
2.14	The stability of the photocatalyst systems	69
CHAPTER THREE- RESULTS AND DISCUSSION: C coated $\text{TiO}_2$		
3.1	Physical Characterization	71
	3.1.1 Elemental and BET analyses	71
	3.1.2 X-ray diffraction (XRD) analysis	75
	3.1.3 X-ray Photoelectron Spectroscopy (XPS) analysis	77
	3.1.4 UV-Vis Diffused Reflectance Spectra (UV-Vis DRS) analysis	81
	3.1.5 SEM and High Resolution Transmittance electron Microscopy (HRTEM) Analysis	83
	3.1.6 Photoluminescence (PL) analysis	87
3.2	Optimization experiments of C coated $\text{TiO}_2$	90
	3.2.1 Effect of carbon content and calcination temperature towards photocatalytic degradation of RR4 dye	90

3.2.2	Effect of the sonication time of C coated TiO <sub>2</sub> towards photocatalytic degradation of RR4 dye	93
3.3	Photocatalytic evaluation of the C coated TiO <sub>2</sub> samples	95
3.3.1	Adsorption and photocatalytic processes under RR4, MB and Phenol	95
3.3.2	Photodegradation of RR4, MB and phenol under different light Irradiations	99
3.4	The operational parameters governing the photocatalytic degradation of RR4 dye by the C-coated TiO <sub>2</sub>	104
3.4.1	Effect of initial dye concentration on the photocatalytic efficiency of C-coated TiO <sub>2</sub>	104
3.4.2	Effect of catalyst loading on the photocatalytic efficiency of C-coated TiO <sub>2</sub>	106
3.4.3	Effect of aeration flow rate on the photocatalytic efficiency of C-coated TiO <sub>2</sub>	108
3.4.4	Effect of initial pH of the RR4 dye solution on the photocatalytic efficiency of C-coated TiO <sub>2</sub>	111
3.5	Mineralization of RR4, MB and phenol by C coated TiO <sub>2</sub>	114
3.6	Stability of the C coated TiO <sub>2</sub>	117
 CHAPTER FOUR- RESULTS AND DISCUSSION: C coated TiO <sub>2</sub> - P25		
4.1	Physical characterization	119
4.1.1	Elemental, BET and HR-TEM analyses	119
4.1.2	X-ray diffraction (XRD) analysis	124
4.1.3	UV-Vis Diffused Reflectance Spectra (UV-Vis DRS) analysis	126
4.1.4	X-ray Photoelectron Spectroscopy (XPS) analysis	128
4.1.5	Photoluminescence (PL) analysis	132
4.2	Optimization experiments of C coated N doped P25	134
4.2.1	Effect of carbon content and calcination temperature towards photocatalytic degradation of RR4 dye	134

4.2.2	Effect of the sonication time in the preparation of C coated TiO <sub>2</sub> -P25 towards the photocatalytic degradation of RR4 dye	136
4.3	Photocatalytic evaluation of the C coated TiO <sub>2</sub> -P25 samples	138
4.3.1	Adsorption and photocatalytic degradation of RR4, MB and Phenol by C coated TiO <sub>2</sub> -P25 TiO <sub>2</sub> samples	138
4.3.2	Photodegradation of RR4, MB and phenol under different light sources.	141
4.4	The operational parameters governing the photocatalytic degradation of RR4 dye by the C coated N doped TiO <sub>2</sub> -P25	147
4.4.1	Effect of initial dye concentration	147
4.4.2	Effect of catalyst loading	150
4.4.3	Effect of aeration flow rate	152
4.4.4	Effect of initial pH	154
4.5	Mineralization study of RR4, MB and Phenol by C coated TiO <sub>2</sub> -P25	157
4.6	The Stability of the photocatalyst	161
<b>CHAPTER FIVE- RESULTS AND DISCUSSION: C coated N doped TiO<sub>2</sub>-P25</b>		
5.1	Physical characterization	163
5.1.1	Elemental and BET analyses	163
5.1.2	X-ray diffraction (XRD) analysis	165
5.1.3	X-ray Photoelectron Spectroscopy (XPS) analysis	167
5.1.4	UV-Vis Diffused Reflectance Spectroscopic (UV-Vis DRS) analysis	171
5.1.5	Transmittance electron Microscopic (TEM) Analysis	173
5.1.6	Photoluminescence (PL) spectroscopic analysis	176
5.2	Optimization in the preparation process of C coated N doped TiO <sub>2</sub> -P25	179
5.2.1	Effect of nitrogen and carbon content and calcination temperature towards photocatalytic degradation of RR4 dye	179
5.3	Photocatalytic evaluation of the C coated N doped TiO <sub>2</sub> -P25 samples	182

5.3.1	Adsorption under RR4, MB and Phenol	182
5.3.2	Photodegradation of RR4, MB and phenol under different light sources	184
5.4	The operational parameters governing the photocatalytic degradation of RR4 dye by the C coated N doped TiO <sub>2</sub>	189
5.4.1	Effect of initial dye concentration on the photocatalytic efficiency of C coated N doped TiO <sub>2</sub> -P25	189
5.4.2	Effect of catalyst loading on the photocatalytic efficiency of C coated N doped TiO <sub>2</sub> -P25	191
5.4.3	Effect of aeration flow rate on the photocatalytic efficiency of C coated N doped TiO <sub>2</sub> -P25	193
5.4.4	Effect of initial pH of the RR4 dye solution on the photocatalytic efficiency of C coated N doped TiO <sub>2</sub> -P25	195
5.5	Mineralization study of RR4 dye, MB and phenol by C coated N doped TiO <sub>2</sub> -P25	198
5.6	The stability of the photocatalyst	200
CHAPTER SIX –SUMMARY: Comparison with related works in the literatures		
6.1	Published works on the C coated TiO <sub>2</sub> photocatalyst in the degradation of RR4, MB and phenol.	202
6.2	Published works on the N doped TiO <sub>2</sub> photocatalysts in the degradation of RR4, MB and phenol.	206
CHAPTER SEVEN- CONCLUSIONS		210
REFERENCES		213
APPENDICES		228
LIST OF PUBLICATIONS AND CONFERENCES		232

## LIST OF TABLES

	Page
Table 1.1: Advanced Oxidation Technologies and other related processes [6].	2
Table 1.2: Redox potentials of some oxidants [7].	3
Table 1.3: Rate constants ( $k$ in $M^{-1}s^{-1}$ ) for some organic compounds with hydroxyl radical and ozone [8].	3
Table 1.4: Different applications of photocatalysis technology [16].	6
Table 3.1: Experimental conditions and results of the carbon coating process of $TiO_2$ . Pseudo first order rate constants ( $k$ ) for the degradation of $30\text{ mg L}^{-1}$ RR4 anionic dye were obtained under low energy Phillips 45 watts fluorescent light irradiation with residual UV leakage of $3.5\text{ W m}^{-2}$ .	72
Table 3.2: Carbon content of C coated $TiO_2$ (TC1-560) upon prolonged irradiations with a 45 W fluorescent lamp in distilled water for 0, 24, 48 and 72 h.	117
Table 4.1: Experimental conditions and results of some characterizations of the C coated $TiO_2$ -P25. Pseudo first order rate constants ( $k$ ) for the degradation of $30\text{ mg L}^{-1}$ RR4 anionic dye were obtained under low energy 45 Watts fluorescent light irradiation with residual UV leakage of $3.5\text{ W m}^{-2}$ .	120
Table 4.2: The binding energy values for each element in carbon coated $TiO_2$ -P25 (PP0.6-450) sample.	131
Table 4.3: Carbon content of C coated $TiO_2$ -P25 upon prolonged irradiations with a 45-W fluorescent lamp in distilled water for 0, 24, 48 and 72 h.	162
Table 5.1: Experimental condition results of the pristine and modified $TiO_2$ -P25. Pseudo first order rate constants ( $k$ ) for the degradation of $30\text{ mg L}^{-1}$ RR4 anionic dye were obtained under low energy Phillips 45 watts fluorescent light irradiation with residual UV leakage of $6.03\text{ W m}^{-2}$ .	164
Table 5.2: The binding energy values for every element in carbon coated nitrogen doped $TiO_2$ -P25 (PU1-350) sample.	170
Table 5.3: Carbon content of C coated N doped $TiO_2$ -P25 upon prolonged irradiations with a 45Watt fluorescent lamp in distilled water for 0, 24, 48 and 72 h.	201

Table 6.1:	Different preparation processes of C coated TiO <sub>2</sub> by other works and its application in the photocatalytic degradation of MB and phenol.	206
Table 6.2:	Different preparation processes of N doped TiO <sub>2</sub> by other works and its application in the photocatalytic degradation of MB and phenol.	209

## LIST OF FIGURES

	Page
Figure 1.1: Earth's light environment (solar spectrum) [17]	7
Figure 1.2: Representation of a city governed by urban photocatalysis, proposed by Italcementi group [18].	7
Figure 1.3: Band gap energy ( $E_g$ ) of the insulator, semiconductor and conductor. CB; conduction band, VB; valance band [19].	9
Figure 1.4: Simplified scheme of semiconductor activation [19].	9
Figure 1.5: Relationship between the band structures of some selected metal oxide and non oxide semiconductors and the redox potentials of water splitting [22].	12
Figure 1.6: Schematic representation of a nanosized photocatalyst particle where the deexcitation process (following the initial irradiation) can occur in four general ways: (A) surface recombination, (B) volume recombination, (C) reduction with electron acceptors, and (D) oxidation with electron donors [19].	12
Figure 1.7: The manufacturing of $TiO_2$ using: a) pyrogenic process, b) precipitation process [25].	15
Figure 1.8: Crystal structure of rutile and anatase in $TiO_2$ [28].	15
Figure 1.9: Molecular orbital structure of anatase: a) atomic levels, b) crystal – field split levels, c) final interaction states [30].	17
Figure 1.10: Overall mechanism involved in $TiO_2$ photocatalyst [25].	20
Figure 1.11: Photoexcitation in composite semiconductor/ semiconductor photocatalyst [19].	30
Figure 1.12: (a) Structure of natural rubber, cis-1, 4-polyisoprene, (b) formation of peroxy formic acid and (c) the production of ENR [92].	34
Figure 1.13: The formation of peat in nature [100].	36
Figure 1.14: The chemical properties in urea [102]	38
Figure 1.15: Molecular structure of RR4 dye [105]	39

Figure 1.16:	The structure of methylene blue [106]	40
Figure 1.17:	The structural of phenol [112]	42
Figure 2.1:	Schematic diagram of the photocatalytic degradation of organic pollutants dye by unmodified and modified TiO <sub>2</sub> under a) lamp, b) solar and c) visible light.	47
Figure 2.2:	The experimental setup for C preparing coated TiO <sub>2</sub> using the calcinations process. (1) Flow meter, (2) muffle furnace (3) stainless or pyrex glass reactor, (4) sample and (5) scrubber.	53
Figure 2.3:	The experimental setup for preparing carbon coated nitrogen doped TiO <sub>2</sub> -P25 using semi closed reactor. (a) Semi closed reactor, (b) Modified photocatalyst sample (c) Muffle furnace and (d) glass tube (semi closed reactor).	55
Figure 3.1:	Fitted straight line curve of the percent carbon content in C coated TiO <sub>2</sub> products prepared at various calcining temperature against the dosage of ENR-50 solution.	74
Figure 3.2:	XRD patterns of the pristine TiO <sub>2</sub> and carbon coated TiO <sub>2</sub> samples prepared at 1.0 g ENR-50 dosage at different calcining temperatures.	76
Figure 3.3:	XPS spectra of (a) the survey spectrum, (b) Ti 2p, (c) O 1s, (d) C 1s and (e) N1s for the carbon coated TiO <sub>2</sub> , TC1-560.	80
Figure 3.4:	UV-Visible diffused reflectance absorption spectra (a) and plots of the transformed Kubelka-Munk function vs the energy of the light absorbed (b) of pristine TiO <sub>2</sub> and carbon coated TiO <sub>2</sub> .	82
Figure 3.5:	SEM micrographs of the (a) pristine TiO <sub>2</sub> and (b) carbon coated TiO <sub>2</sub> , TC1-560.	84
Figure 3.6	TEM images of (a) TiO <sub>2</sub> (b) carbon coated TiO <sub>2</sub> , HRTEM images of carbon coated TiO <sub>2</sub> , TC1-560 (c and d).	86
Figure 3.7	Photoluminescence spectra of (a) pristine TiO <sub>2</sub> and carbon coated TiO <sub>2</sub> with different calcination temperature but similar C content and (b) pristine TiO <sub>2</sub> and carbon coated TiO <sub>2</sub> prepared at 560 °C containing different amount of carbon (refer Table 2).	89

Figure 3.8	Plots of the pseudo first order rate constants (k) for the degradation of 30 mg L <sup>-1</sup> RR4 under a 45 W fluorescent lamp for carbon coated TiO <sub>2</sub> prepared at different calcining temperatures and containing different carbon content.	92
Figure 3.9	The effect of sonication time of the solution mixture on the photocatalytic activity of the photocatalysts (TC1-560).	94
Figure 3.10:	The effect of carbon content on the pseudo first order rate constants in the photocatalytic degradation of the various organic pollutants under a 45 W fluorescent lamp by carbon coated TiO <sub>2</sub> samples (TC1-560).	97
Figure 3.11:	The effect of different light sources on the photocatalytic activities of the pristine TiO <sub>2</sub> and TC1-560 photocatalysts in the degradation of (a) 30 mg L <sup>-1</sup> RR4, b) 12 mg L <sup>-1</sup> MB (b) and (c) 10 mg L <sup>-1</sup> phenol solution.	103
Figure 3.12:	Photocatalytic degradation at different initial concentration of RR4 using C coated TiO <sub>2</sub> sample (TC1-560) under a 45 W fluorescence lamp.	105
Figure 3.13:	Pseudo first order rate constant of photocatalytic degradation of 20 mL RR4 dye at different amount of TC1-560 loading irradiated with a 45 Watt fluorescent lamp.	107
Figure 3.14:	Effect of aeration flow rate on the photocatalytic degradation of 30 mg L <sup>-1</sup> RR4 by TC1-560 under a 45 W fluorescent lamp.	110
Figure 3.15:	Photocatalytic degradation of different pH of RR4 dye under TC1-560 sample irradiated with a 45 Watt fluorescent lamp.	112
Figure 3.16:	Point of zero charge for C coated TiO <sub>2</sub> (TC1-560).	113
Figure 3.17:	COD values for photodegradation of RR4, MB and phenol using pristine TiO <sub>2</sub> and TC1-560 irradiated with a 45 Watt fluorescent lamp.	116
Figure 3.18:	Photocatalytic efficiency of TC1-560 carbon coated TiO <sub>2</sub> upon recycled applications in the (a) degradation of RR4 and (b) its DRS UV-Vis spectra before and after the 5 <sup>th</sup> cycle of application.	118

Figure 4.1:	TEM images for: a) HRTEM images for carbon coated in the surface of P25 for sample carbon coated nitrogen doped TiO <sub>2</sub> -P25, b) TEM image for pristine TiO <sub>2</sub> -P25 and c) TEM image for carbon coated nitrogen doped TiO <sub>2</sub> -P25	123
Figure 4.2:	XRD patterns of the pristine P25 and C coated TiO <sub>2</sub> -P25 samples prepared at 0.6 g peat coagulant dosage at different calcination temperatures.	125
Figure 4.3:	UV-Visible diffused reflectance absorption spectra (a) and plots of the transformed Kubelka-Munk function versus the energy of the light absorbed (b) of pristine TiO <sub>2</sub> -P25 and C coated TiO <sub>2</sub> -P25.	127
Figure 4.4:	XPS spectra of (a) Ti2p, (b) O1s, (c) N1s and (d) C1s for the C coated TiO <sub>2</sub> -P25 (PP0.6-450).	130
Figure 4.5:	Photoluminescence spectra of pristine P25 and C coated TiO <sub>2</sub> -P25 prepared at 450 °C containing different amount of peat loading.	133
Figure 4.6:	Pseudo first order rate constant for the degradation of 30 mg L <sup>-1</sup> RR4 dye under different amount of peat modified TiO <sub>2</sub> -P25 represent by different amount of peat at various calcinations temperature.	135
Figure 4.7:	The effect of sonication time of the solution mixture on the photocatalytic activity of the photocatalysts.	137
Figure 4.8:	Adsorption study for pristine TiO <sub>2</sub> -P25 and PP0.6-450 for various types of pollutants for 1 hour of adsorption process.	139
Figure 4.9:	Photocatalytic degradation of the pollutants: (a) 30 mg L <sup>-1</sup> RR4, (b) 12 mg L <sup>-1</sup> MB and (c) 10 mg L <sup>-1</sup> phenol using presaturated PP0.6-450 and normal PP0.4-450.	140
Figure 4.10:	Photocatalytic degradation of various type pollutants: (a) RR4, (b) MB and (c) phenol under pristine TiO <sub>2</sub> -P25 and PP0.6-450 at different types of irradiation.	146
Figure 4.11:	Effect of different concentration in terms of: (a) photodegradation of RR4, (b) pseudo first order rate constant of RR4 using PP0.6-450 sample and (c) the observation of the color intense for RR4 at different concentration.	149

Figure 4.12:	Pseudo first order rate constant of the degradation 20 mL of RR4 dye at different loading of PP0.6-450 sample.	151
Figure 4.13:	Effect of aeration flow rate on the photocatalytic degradation of 30 mg L <sup>-1</sup> RR4 by PP0.6-450 under a 45 W fluorescent lamp.	153
Figure 4.14:	Photocatalytic degradation at different pH of RR4 dye under PP0.6-450 sample irradiated with 45 Watt fluorescent lamp.	155
Figure 4.15:	Point of zero charge for C coated TiO <sub>2</sub> -P25, PP0.6-450.	156
Figure 4.16:	TOC values for photodegradation of RR4, MB and phenol using pristine TiO <sub>2</sub> -P25 and PP0.6-450 irradiated with 45 Watt fluorescent lamp.	159
Figure 4.17:	HPLC chromatogram for a) RR4, b) phenol with intermediates respectively.	160
Figure 4.18:	Photocatalytic efficiency of PP0.6-450, C coated TiO <sub>2</sub> -P25 upon recycled applications in the degradation of RR4.	162
Figure 5.1:	XRD patterns of the pristine TiO <sub>2</sub> -P25 and C coated N doped TiO <sub>2</sub> -P25 samples prepared at 0.6 g urea dosage at different calcining temperatures.	166
Figure 5.2:	XPS spectra of (a) Ti 2p, (b) O 1s (c) N 1s and (d) C 1s for the C coated N doped TiO <sub>2</sub> -P25 (PU1-350).	169
Figure 5.3:	UV-Visible diffused reflectance of: (a) absorption spectra of pristine P25 and C coated N doped TiO <sub>2</sub> -P25, (b) plots of the transformed Kubelka-Munk function vs the energy of the light absorbed.	172
Figure 5.4:	TEM images of (a) P25 (b) C coated N doped TiO <sub>2</sub> -P25, HRTEM images of C coated N doped TiO <sub>2</sub> -P25, PU1-350 (c and d).	175
Figure 5.5:	Photoluminescence spectra of (a) pristine P25 and C coated N doped TiO <sub>2</sub> -P25 with different calcination temperature but similar amount of urea and (b) pristine P25 and C coated N doped TiO <sub>2</sub> -P25 prepared at 350 °C containing different amount of Urea (refer Table 5.1).	177

Figure 5.6:	Plots of the pseudo first order rate constants ( k) for the degradation of 30 mg L <sup>-1</sup> RR4 under 45-W fluorescent lamp for C coated N doped TiO <sub>2</sub> -P25 prepared at different calcining temperatures and containing different amount of C and N.	181
Figure 5.7:	Adsorption study of pristine TiO <sub>2</sub> -P25 and PU1-350 under RR4, MB and phenol in 1 hour of irradiation.	183
Figure 5.8	Plots of the photocatalytic degradation of 30, 12 and 10 mg L <sup>-1</sup> of RR4, MB and phenol respectively, under pre-saturated PU1-350 (photo-catalysis) and normal PU1-350 (ads + photo-catalysis) under 45 Watt fluorescent lamp.	183
Figure 5.9	The effect of different light sources on the photocatalytic activities of the pristine TiO <sub>2</sub> -P25 and PU1-350 photocatalysts in the degradation of (a) 30 mg L <sup>-1</sup> RR4, b) 12 g L <sup>-1</sup> MB (b) and (c) 10 mg L <sup>-1</sup> phenol solution under 45-W fluorescent lamp and (a) 60 mg L <sup>-1</sup> RR4 , b) 36 mg L <sup>-1</sup> MB (b) and (c) 30 mg L <sup>-1</sup> phenol solution under solar irradiation.	187
Figure 5.10	Photocatalytic degradation at different initial concentration of RR4 using C coated N doped TiO <sub>2</sub> -P25 sample (PU1-350).	190
Figure 5.11:	Pseudo first order rate constant for the photocatalytic degradation of 20 mL RR4 dye by different amount of PU1-350 loading irradiated with a 45 Watt fluorescent lamp.	192
Figure 5.12:	Effect of aeration flow rate on the photocatalytic degradation of 30 mg L <sup>-1</sup> of RR4 with PU1-350 as a photocatalyst under a 45 W fluorescent lamp.	194
Figure 5.13:	Photocatalytic degradation at different pH of RR4 dye under PP0.6-450 sample irradiated with 45 Watt fluorescent lamp.	196
Figure 5.14:	Point of zero charge for C coated N doped TiO <sub>2</sub> -P25 (PU1-350).	197
Figure 5.15:	TOC values for photodegradation of RR4, MB and phenol using pristine P25 and PU1-350 irradiated with 45 Watt fluorescent lamp.	199
Figure 5.16:	Photocatalytic efficiency of PU1-350, C coated N doped TiO <sub>2</sub> -P25 upon recycled applications in the degradation of RR4 irradiated with 45 Watt fluorescent lamp.	201

## LIST OF ABBREVIATIONS

a.u	Arbitrary units
AOPs	Advance oxidation processes
CHN	Carbon, Hydrogen, Nitrogen
COD	Chemical Oxygen Demand
CB	Conduction Band
$e^-$	Negative electron
$E_{bg}$	Energy band gap
$h^+$	Positive hole
h $\nu$	Photonic energy
LUMO	Lowest unoccupied molecular orbital
MB	Methylene Blue dye
HUMO	Highest unoccupied molecular orbital
HRTEM	High Resolution Transmission Electron Microscopy
PL	Photoluminescence
RR4	Reactive Red 4 dye
SEM	Scanning Electron Microscopy
TOC	Total Organic Compounds
UV	Ultraviolet
UV-VIS DRS	UV-Visible diffuse reflectance spectroscopy
VB	Valence band

**SINTESIS DAN PENCIRIAN TiO<sub>2</sub> TERSALUT KARBON DAN TERDOP  
NITROGEN BAGI PENINGKATAN PENGURAIAN  
PEMFOTOMANGKINAN KE ATAS BAHAN CEMAR ORGANIK DI  
BAWAH SINARAN CAHAYA UV-VIS DAN NAMPAK**

**ABSTRAK**

TiO<sub>2</sub> komersial yang murah dan sedia ada dipasaran iaitu TiO<sub>2</sub> (99% anatase ) dan TiO<sub>2</sub>-P25 (80% anatase dan 20% rutil) telah diubahsuai untuk menghasilkan TiO<sub>2</sub> terdop karbon (C) dan nitrogen (N) bagi meningkatkan fotoaktiviti bahan tersebut dibawah sinaran cahaya UV dan cahaya nampak. Modifikasi fotopemangkin ini dijalankan dengan menggunakan polimer semulajadi iaitu ENR-50 dan penggumpal tanah gambut (peat) sebagai prekursor karbon sementara urea digunakan sebagai prekursor nitrogen dan karbon. TiO<sub>2</sub> terubahsuai dengan menggunakan ENR-50 menghasilkan TiO<sub>2</sub> terdop C. Keadaan optimum bagi C adalah 1 g larutan ENR-50 dan 560°C bagi suhu kalsinasi untuk menghasilkan sampel optimum terdop C yang mengandungi sebanyak 0.25% C dengan lapisan ketebalan 0.68 nm. Dengan menggunakan pencelup reaktif merah 4 (RR4) sebagai model bahan cemar, kadar penguraian foto bagi C terdop TiO<sub>2</sub> optimum menjadi 3.7 dan 5.5 kali ganda lebih cepat berbanding TiO<sub>2</sub> asal masing-masing di bawah sinaran 45 W lampu kalimantang dan solar. Lapisan C yang terdapat pada TiO<sub>2</sub> adalah penyebab meningkatnya kadar penguraian foto kerana ia bertindak sebagai pengaut elektron. Walaubagaimanapun, tiada kesan penguraian pemfotomangkinan dapat dilihat di bawah cahaya nampak disebabkan tenaga luang jalur yang melebihi 3.0 eV.

TiO<sub>2</sub>-P25 terubahsuai dengan penggumpal tanah gambut menghasilkan lapisan C berketebalan 0.34 nm dimana kandungan N yang sedikit juga dikesan. Keadaan optimum untuk TiO<sub>2</sub>-P25 tersalut C adalah sebanyak 0.4 g larutan penggumpal tanah gambut pada kalsinasi suhu 450 °C. TiO<sub>2</sub>-P25 tersalut karbon yang optimum telah meningkatkan fotoaktiviti penguraian pencelup RR4 dengan ketara berbanding TiO<sub>2</sub>-P25 asal di bawah sinaran 45 W lampu kalimantang dan solar dan ia juga menunjukkan sedikit respon fotoaktiviti terhadap sinaran cahaya nampak.

TiO<sub>2</sub>-P25 terubahsuai menggunakan urea menghasilkan TiO<sub>2</sub>-P25 tersalut C dengan lapisan C berketebalan 2.04 nm sementara N terdop sebagai Ti-N bagi menukarganti tempat oksigen dalam pemangkin. Keadaan optimum bagi modifikasi fotopemangkin ini adalah 1 g urea dan 350°C pada suhu kalsinasi. Fotoaktiviti yang baik dapat diperhatikan dengan sebanyak 90% pengelup RR4 dapat disingkirkan dengan hanya 5 minit diiradiasikan dibawah 45 W lampu kalimantang. C tersalut N terdop TiO<sub>2</sub>-P25 menunjukkan respon yang sangat bagus dibawah sinaran cahaya nampak dengan menyelesaikan tugas kurang dari 120 minit penguraian terhadap pencelup RR4, sementara tiada kesan penguraian pemfotomangkinan yang dapat dilihat dengan menggunakan TiO<sub>2</sub>-P25 asal dibawah kondisi yang sama. Kesan sinergi bagi setiap modifikasi fotopemangkin diterokai dengan menggunakan SEM, HRTEM, XPS, BET, UV-Vis-DRS, CHN dan spektroskopi fotopendarcahaya. Penilaian terhadap fotopemangkin bagi sampel juga dijalankan dengan menggunakan metilena biru (MB) dan fenol sebagai bahan cemar kedua dan ketiga. Kesan terhadap parameter operasi seperti kesan muatan pemangkin, kadar aliran udara dan pH awal adalah masing –masing 0.02 g, 25 mL min<sup>-1</sup> dan pH 7. Kesemua fotopemangkin terubahsuai adalah stabil terhadap sinaran yang lama dan aktiviti foto juga konsisten sehingga 5 kitaran ulang guna.

# **SYNTHESIS AND CHARACTERIZATION OF CARBON COATED AND NITROGEN DOPED TiO<sub>2</sub> FOR ENHANCED PHOTOCATALYTIC DEGRADATION OF ORGANIC POLLUTANTS UNDER UV-VIS AND VISIBLE LIGHT IRRADIATION**

## **ABSTRACT**

A commercially available and relatively cheap TiO<sub>2</sub> (99% anatase) and TiO<sub>2</sub>-P25 (80% anatase and 20% rutile) were modified to produce carbon (C) and nitrogen (N) incorporated TiO<sub>2</sub> to improve its photoactivity under UV-Vis and visible light regions. Both the TiO<sub>2</sub> and TiO<sub>2</sub>-P25 were modified using natural polymers of ENR-50 and peat coagulant (peat) as carbon precursor while urea was used as N and C precursor. TiO<sub>2</sub> modified with ENR-50 produced a C coated TiO<sub>2</sub>. The optimum condition for C coating was 1.0 g ENR-50 solution and 560 °C of calcination temperature to yield the optimum C coated sample containing 0.25 % C with a C layer thickness of 0.68 nm. By using Reactive Red 4 dye (RR4) as model pollutant, the photocatalytic degradation rate of the optimum C coated TiO<sub>2</sub> was 3.7 and 5.5 times faster than that of the pristine TiO<sub>2</sub> under 45 W fluorescent lamp and solar irradiations respectively. The C layer present in TiO<sub>2</sub> was responsible for increasing its photoactivity by acting as an electron scavenger. However, no photocatalytic degradation was observed under visible light irradiation for all C coated TiO<sub>2</sub> due to their bandgap energy (E<sub>g</sub>) values higher than 3.0 eV.

TiO<sub>2</sub>-P25 modified with peat coagulant produced a 0.34 nm thickness of C layer coated on its surface where a low amount of N was also detected. The optimum condition for C coated TiO<sub>2</sub>-P25 was at 0.4 g of peat coagulant solution

loading using 450°C of calcination temperature. The optimum C coated TiO<sub>2</sub>-P25 significantly increased the photocatalytic degradation of RR4 dye as compared with pristine TiO<sub>2</sub>-P25 under a 45-W fluorescent lamp and solar light and also indicates low photocatalytic activity under visible light irradiation.

TiO<sub>2</sub>-P25 modified with urea produced a photocatalyst coated with 2.04 nm C thickness while N was doped as Ti-N where it substituted the site of oxygen atom of the catalyst. The optimum preparation for this modified photocatalyst was at 1 g of urea and 350°C of calcination temperature. A good photocatalytic activity was observed where 90% of RR4 dye was removed by the optimum C coated N doped TiO<sub>2</sub>-P25 in only 5 minutes of irradiation under a 45 W fluorescent lamp. The bandgap energy for C coated N doped P25 was reduced to 2.6 eV. It demonstrated impressive photocatalytic activity under visible light irradiation by degrading the RR4 dye entirely in less than 120 minutes. Meanwhile, no photocatalytic degradation was observed using pristine P25 under the same condition. The synergistic effects of each modified photocatalysts were examined using SEM, HRTEM, XPS, BET, UV-Vis-DRS, CHNS and photoluminescent analyses. The photocatalytic evaluation of the samples was also carried out using methylene blue (MB) and phenol as the second and third pollutants. The operational parameters for all modified photocatalysts such as effect of catalyst loading, aeration flow rate and initial pH were found to be optimum at 0.02 g, 25 mL min<sup>-1</sup> and pH 7 respectively. All the modified photocatalysts were stable upon exposure to the long duration of irradiation and their photoactivity activities were consistent up to the 5<sup>th</sup> cycle of reuse.

# CHAPTER 1

## INTRODUCTION

### 1.1 Environmental Problems

Environmental pollution, such as contaminated water or polluted air, has become a global issue threatening the health of mankind. Typical polluting sources are toxic organic molecules or hazardous gas compounds which are released from household waste, livestock waste and local industries. Science is thus involved in searching for new alternatives and ecologically sustainable techniques for cleaning up the environmental contamination [1]. Different solutions for solving these problems have already been proposed such as air scrubbing, adsorption etc., but some of them only remove the pollutant from one phase to another and then require additional processes to eliminate the toxic compounds [2].

### 1.2 Advance Oxidation Process (AOP)

Advanced oxidation processes (AOPs) are efficient novel methods for water treatment that have produced very good results in industrialized countries and are beginning to be employed in the developing regions [3-5]. AOPs are based on physicochemical processes that produce profound changes in the structure of chemical species. The concept was initially established by Glaze et al. [4], who defined AOPs processes as those involving generation and use of powerful transitory species especially hydroxyl radical ( $\text{HO}^\bullet$ ). This species can be generated by photochemical process (solar light) or by other forms of energy, and has a high efficiency for organic matter oxidation [5]. Some AOPs, such as heterogeneous photocatalysis, radiolysis and others, can also produce reducing agents, allowing the transformation of pollutants that are difficult to oxidize such as some metal ions or

halogenated compounds into safer species. AOPs are usually divided into non-photochemical and photochemical processes, as listed in Table 1.1.

Table 1.1: Advanced Oxidation Technologies and other related processes [6].

Non-photochemical processes	Photochemical processes
Alkaline ozonation ( $O_3/OH^-$ )	Water photolysis in vacuum ultraviolet (VUV)
Ozonation with hydrogen peroxide ( $O_3/H_2O_2$ )	UV/hydrogen peroxide
Fenton and related processes ( $Fe^{2+}/H_2O_2$ )	UV/ $O_3$
Electrochemical oxidation processes	Photo-Fenton
$\gamma$ -Radiolysis and electron-beam treatment	UV/periodate
Non-thermal plasma	Heterogeneous photocatalysis
Electrohydraulic discharge—ultrasound	
Oxidation in sub/and supercritical water	
Zero-valent iron	
Ferrate ( $K_2FeO_4$ , Fe(VI))	

The high efficiency of AOPs is supported on thermodynamic and kinetic grounds, due to the participation of radicals. The hydroxyl radical can attack virtually all organic compounds and it reacts 10<sup>6</sup>–10<sup>12</sup> times more rapidly than alternative oxidants such as ozone ( $O_3$ ) [5]. From Table 1.2, it can be observed that, after fluorine, hydroxyl radical ( $OH^\bullet$ ) is the most energetic oxidant due to its high redox potential (high redox potential means strong oxidant agent species).

Table 1.3 shows that the reaction rate constant of different compounds with  $\text{OH}^\bullet$  are several orders of magnitude higher than those with  $\text{O}_3$ . Another active oxygen species is the superoxide radical ( $\text{O}_2^{\bullet -}$ ) and its conjugate acid from the hydroperoxyl radical ( $\text{HO}_2^\bullet$ ). These radicals are also produced in many AOPs, but they are far less active than  $\text{OH}^\bullet$  since as indicated in Table 1.2, their redox potentials are lower than that of  $\text{OH}^\bullet$  radical.

Table 1.2: Redox potentials ( $E^0$ ) of some oxidants [7].

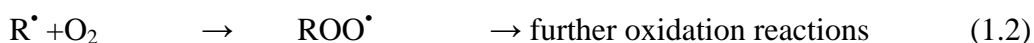
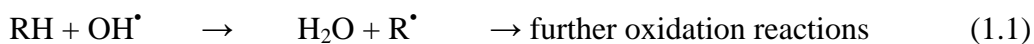
Species	$E^0(\text{V}, 25^\circ\text{C})^1$
Fluorine	3.03
Hydroxyl radical	2.80
Atomic oxygen	2.42
Ozone	2.07
Hydrogen peroxide	1.78
Perhydroxyl radical/ Hydroperoxyl radical	1.70
Permanganate	1.68
Chlorine dioxide	1.57
Hypochlorous acid	1.49
Chlorine	1.36
Bromine	1.09
Superoxide radical	0.59
Iodine	0.54

<sup>1</sup>: Redox potentials referred to normal hydrogen electrode (NHE)

Table 1.3: Rate constants ( $k$  in  $\text{M}^{-1} \text{s}^{-1}$ ) for some organic compounds with hydroxyl radical and ozone [8].

Compound	Rate constant ( $\text{M}^{-1} \text{s}^{-1}$ )	
	$\text{OH}^\bullet$	$\text{O}_3$
Chlorinated alkenes	$10^9 - 10^{11}$	$10^{-1} - 10^3$
Phenols	$10^9 - 10^{10}$	$10^3$
Aromatics	$10^8 - 10^{10}$	$1 - 10^2$
Ketones	$10^9 - 10^{10}$	1
Alcohols	$10^8 - 10^9$	$10^{-2} - 1$
Alkanes	$10^6 - 10^9$	$10^{-2}$

When a target pollutant compound is attacked by  $\text{OH}^\bullet$ , three main mechanisms may be involved in the degradation of organics: hydrogen abstraction,  $\text{OH}^\bullet$  addition or substitution and electron transfer. Hydrogen abstraction is generally the first step in many acid compounds [5, 7, 8]:



AOPs are developed and commercialized to a variable degree and are undergoing constant change as technological advances take place. At present, UV/ $\text{H}_2\text{O}_2$ , UV/ $\text{O}_3$ , UV/ $\text{H}_2\text{O}_2/\text{O}_3$ , photo fenton and heterogeneous photocatalysis (UV/ $\text{TiO}_2$ ) are commercialized [6].

### 1.3 Heterogeneous Photocatalysis

The words “photocatalyst” is Greek origin and composed from two parts: the “photo” (light) and the word “catalysis” (decomposed). Although there was no consensus in the scientific community as to proper definition of photocatalyst, the term generally can be used to describe the active substance under light irradiation [9]. The photocatalysis is the process to enhance the rate of a chemical reaction in the presence of light without being involved itself in the chemical transformation. Thus, the main difference between a conventional thermal catalyst and photocatalyst is that the former is activated by the heat whereas the latter is activated by photons from the light to appropriate energy. Photocatalytic reactions may occur homogeneously or heterogeneously, but heterogeneous photocatalysts is more intensively studied in

recent years because of its potential use in a variety of environmental and energy-related applications as well as organic synthesis [10].

Heterogeneous photocatalysis is a potential process that has been focused since the early 1970s, when Fujishima and Honda discovered the photocatalytic splitting of water on TiO<sub>2</sub> electrodes [11]. This technique is considered to be one of the most promising Advanced Oxidation Process (AOPs) because of its specific advantages. Heterogeneous photocatalysis is based on the interaction between semiconductor materials and photon from light. By considering that we can get 'free' light from the sun, the idea of using solar light energy as a resource to clean up the environment is an ideal and extremely promising approach. Sun light is a clean and renewable energy source that is readily available. Before reaching the Earth's surface, a part of the solar energy is absorbed by the stratosphere, ozonosphere and other atmospheric layers [12].

Solar radiation reaching the Earth with 5 and 43% of UV and visible light respectively, with the remaining part (52%) is composed of infrared and longer wavelengths radiation (Figure 1.1). Approximately 40% of the total amount of radiation arriving on Earth is mainly composed of visible, infrared, and radio energies. In case of ultraviolet (UV) light, it is generally divided into three regions namely UV-A (315 – 400 nm), UV-B (280 – 315 nm) and UV-C (100 – 280 nm) [13], which is responsible for most of the photochemical processes occurring in the atmosphere. UV-C radiance is mostly filtered by Earth's ozone layer, UV-A and UV-B radiations still pass and have the potential to generate photochemical processes such as the synthesis of vitamin D. However, long term exposure to UV light is very dangerous to human body since it probably can cause skin damage and cancer [14]. The development of photocatalytic technology under different application is

illustrated in Table 1.4. In its early age, a revolutionary idea of cleanliness was suggested by the great Japanese ‘fathers’ of this field [15]. In the past, ‘light cleaning’ means ‘a fast job (a quick wipe-up or dusting)’, but in the future it will mean ‘cleaning with light’. The representation of a city with complete self cleaning technology is depicted in Figure 1.2.

Table 1.4: Different applications of photocatalysis technology [16].

<b>Property</b>	<b>Category</b>	<b>Application</b>
Self-cleaning	Material for residential and office buildings	Exterior tiles, kitchen bathroom components, interior furnishing, plastic surface, building stone
	Indoor and Outdoor lamps and related systems	Translucent paper for indoor lamp covers, coating on fluorescent lamp and highway tunnel lamp cover glass
	Materials for roads	Tunnel wall, sound proofed wall, traffic signs and reflectors
	Others	Tent material, clothes for hospital garments and uniforms and spray coating for cars
Air- cleaning	Indoor air cleaners	Room air cleaner, photocatalyst-equipped air conditioners and interior air cleaner for factories
	Outdoor air purifiers	Concrete for highways, roadways and building
Water purification	Drinking water	River water, groundwater, lakes and water storage tanks
	Others	Fish feeding tanks, drainage water and industrial wastewater
Antitumor activity Cancer therapy		Endoscopic-like instruments
Self-sterilizing	Hospital	Tiles to cover the floor walls of operating rooms, silicone rubber for medical catheters and hospital garments and uniforms
	Others	Public rest rooms, bathrooms

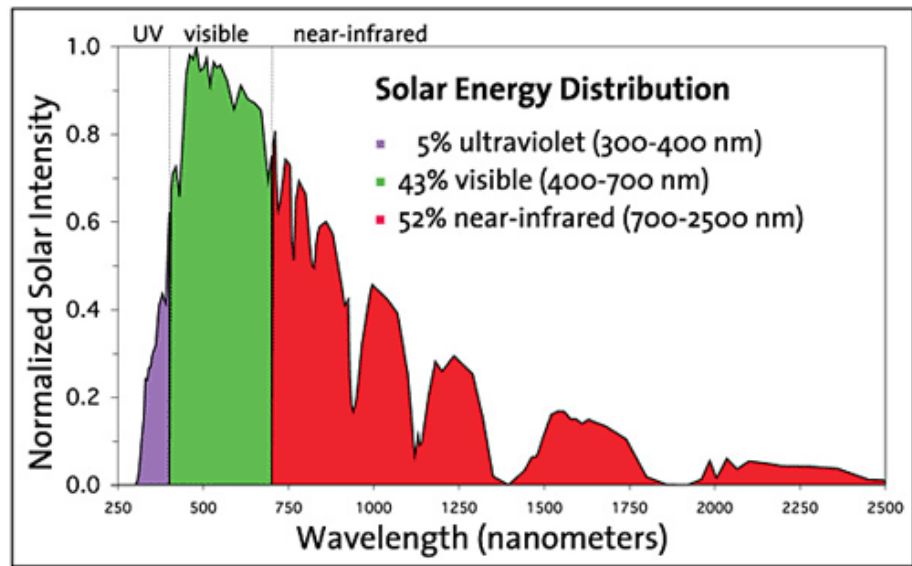


Figure 1.1: Earth's light environment (solar spectrum) [17].

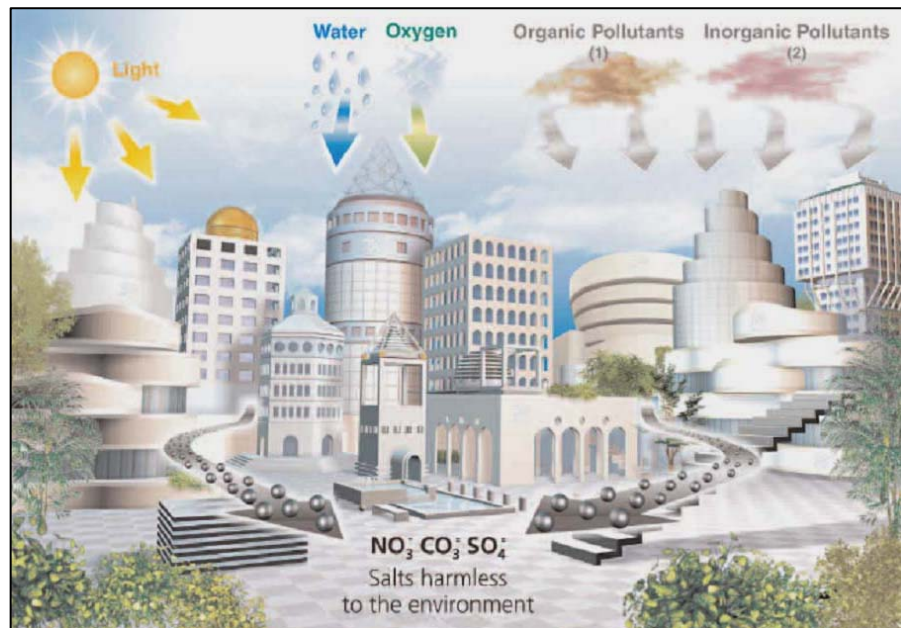


Figure 1.2: Representation of a city governed by urban photocatalysis, proposed by Italcementi group [18].

#### 1.4 Principles of semiconductor photocatalysis

Semiconductors are particularly useful as photocatalyst because of a favorable combination of electron structure, light absorption properties, charge transport characteristics and excited state lifetime [19]. The electron characteristics of conductors, semiconductors and insulators can be described accordingly via the band theory. The corresponding energy levels are so closely spaced that they form bands because of the large number of atoms interact in a solid material. Each band has a different energy and the electrons fill from the lowest to the highest energy and it is similar to the way that electrons occupy the orbitals in a single atom. The highest energy filled band, which is analogous to the 'Highest Occupied Molecular Orbital' (HOMO) in a molecule, is called the valence band (VB). The next higher band, which is analogous to the 'Lowest Unoccupied Molecular Orbital' (LUMO) in the molecule, is called the conduction band (CB). The VB and CB are separated by the band gap ( $E_{bg}$ ). The size of  $E_{bg}$  for each material can be determined for the conductor, semiconductor or insulator as can be seen in Figure 1.3. In general, for electron to flow in a solid under the application of an electric field, they must be in a partially filled band or have access to a nearby empty band [19,20]. In Figure 1.3, there is no possibility of electron flow for insulator because the valence band is completely filled with electrons and the conduction band is too far away in energy to be accessed by these electrons. For a conductors like metals, valence band overlaps with conduction band. Thus, the electrons can access empty areas within the valence band and move freely across all atoms in metal. For a semiconductor, there is a special case in which the band gap is small enough (generally less than 4 eV) that can be bridged either by heat or light to promote electron from the VB to the CB. The mechanism of a semiconductor activated by light is illustrated in Figure 1.4.

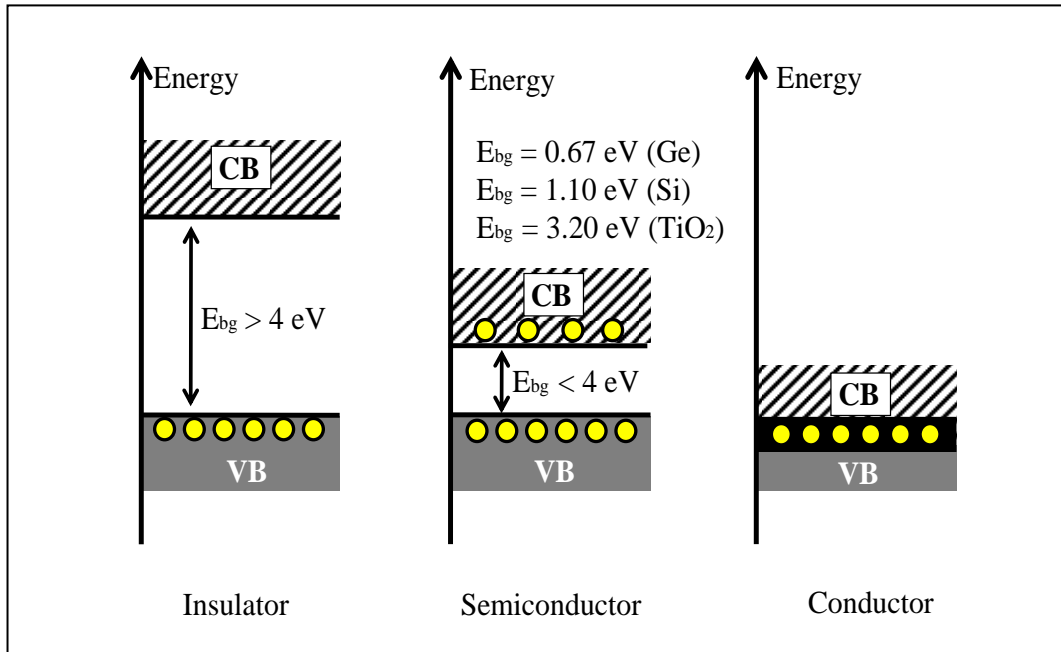


Figure 1.3: Band gap energy ( $E_g$ ) of the insulator, semiconductor and conductor. CB; conduction band, VB; valance band [19].

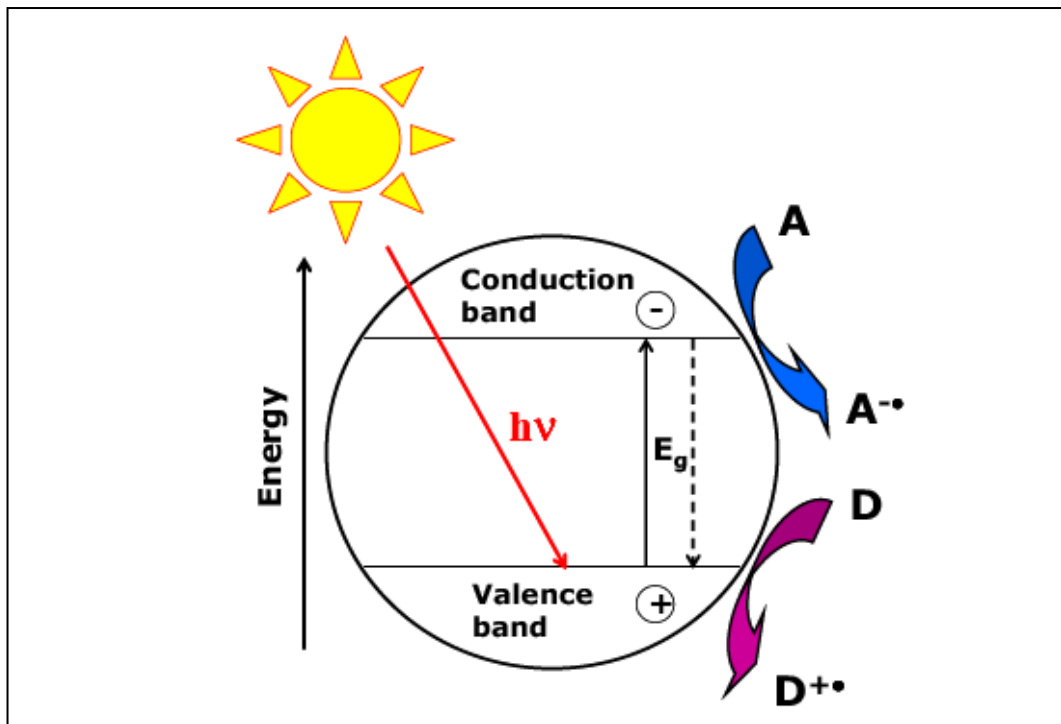


Figure 1.4: Simplified scheme of semiconductor activation [19].

Activation of a semiconductor photocatalyst is achieved through the absorption of a photon into its bandgap energy which results in the promotion of an electron from the VB into the CB, with the concomitant generation of a hole in the valence band. For an example, when a semiconductor is used as a photocatalyst in the environmental remediation, it should be capable to generate a valence band hole with a redox potential that is positive enough to oxidize the organic pollutant. At the same time the photogenerated electron in the conduction band should be negative enough to reduce adsorbed O<sub>2</sub> to superoxide radical anion [21]. The probability and the rate of charge transfer processes depend on the position of the conduction and valence band edges and on the redox potentials of the adsorbed species [19].

Figure 1.5 shows the band gap values of different semiconductors and their position on the electrochemical scale. A substrate can successfully interact only with some semiconductors, it is necessary that the electrochemical potential value of the electron acceptor is more positive (down in the graph) than the semiconductor conduction band potential, and that the electron donor potential is more negative (up in the graph) than that of the semiconductor valence band. A photocatalytic reaction can take place only under such conditions. Recombination of electron-hole pairs can occur in competition with a charge transfer to adsorbed species [21] as shown in Figure 1.6. This phenomenon represents the major deactivation path which could significantly decrease the photocatalytic efficiency. The detrimental process of back-donation to the semiconductor after charge transfer to the adsorbed species can also occur.

The main reaction scheme of a photocatalytic process can be summarized in the following equations (1.3-1.12).

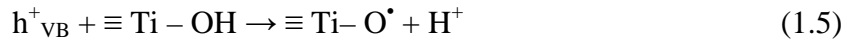
a) Charge separation



b) Bulk/surface recombination



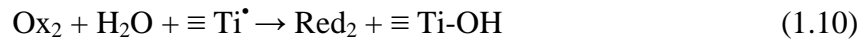
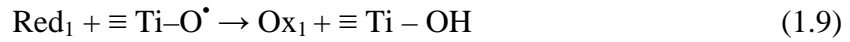
c) Surface trapping



d) Surface recombination



e) Interfacial charge transfer



f) Back reaction



The process of photocatalytic reaction by  $\text{TiO}_2$  takes place by the absorption of ultraviolet (UV) or near-ultraviolet photons ( $h\nu$ ) that is equal or exceed the band gap energy ( $E_g$ ) value for anatase 3.2 eV, or 3.0 eV for rutile onto its surface. An electron would be photoexcited from the valence band (VB) to the empty conduction band (CB) of the  $\text{TiO}_2$  and a positive hole would be left in the valence band in femtoseconds ( equations 1.3). Surface trapping of the induced charges could also occur via equations 1.5-1.6. Subsequently, various possible reactions could occur

such as charge recombination ( equation 1.4 and 1.7-1.8) and a series of reductive and oxidative reactions will be induced on the  $\text{TiO}_2$  surface ( equations 1.9 -1.12).

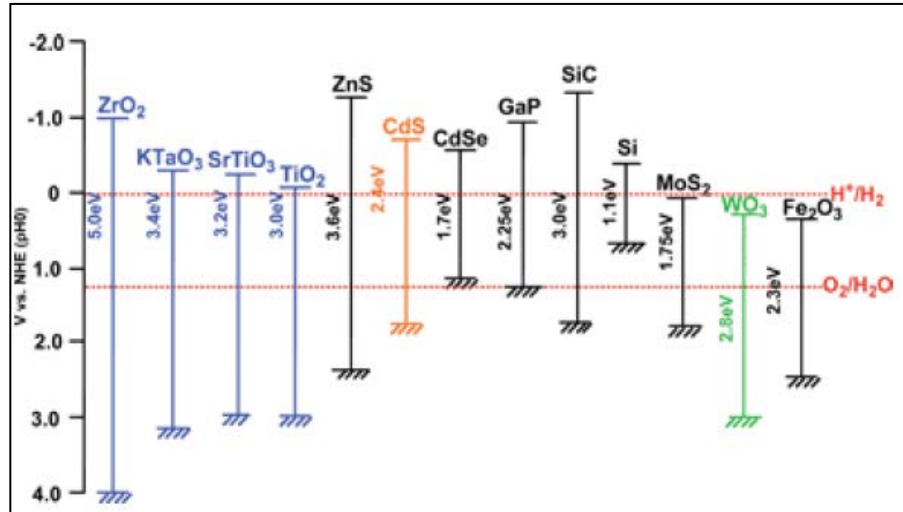


Figure 1.5: Relationship between the band structures of some selected metal oxide and non oxide semiconductors and the redox potentials of water splitting [22].

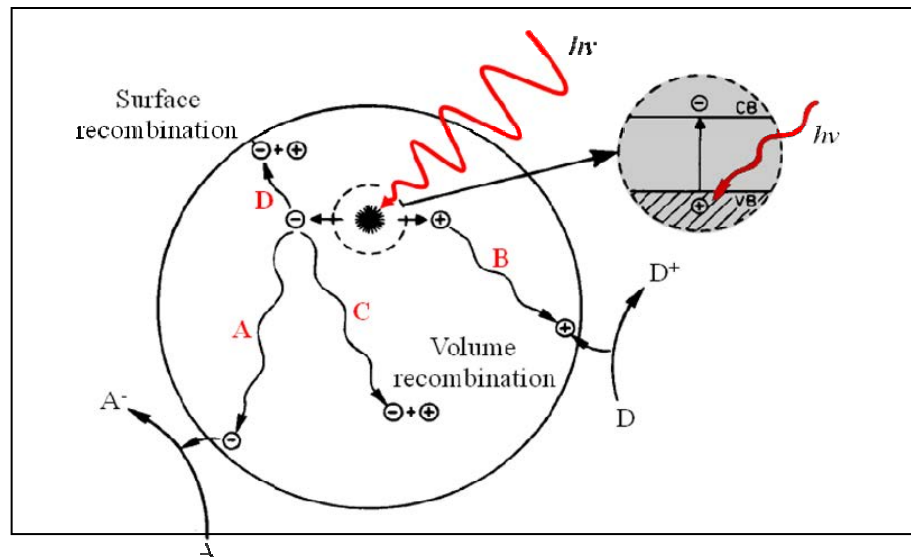


Figure 1.6: Schematic representation of a nanosized photocatalyst particle where the deexcitation process (following the initial irradiation) can occur in four general ways : (A) surface recombination, (B) volume recombination, (C) reduction with electron acceptors, and (D) oxidation with electron donors [19].

## 1.5 TiO<sub>2</sub> as photocatalyst

Any common catalytic material is not consumed during the course of a chemical reaction. Similarly, a photocatalyst must be stable and not tend to decompose due to long exposure to light. In addition, a good photocatalyst must be:

- photoactive
- able to absorb visible and/or near UV light
- biologically and chemically inert
- photostable (*i.e.* not liable to photoanodic corrosion)
- inexpensive
- non-toxic

In many cases, the semiconductor itself risks to incur oxidative decomposition by the photogenerated holes. Generally, only *n-type* semiconductor oxides are stable towards photoanodic corrosion, although such oxides usually have large band gap energy which means that the semiconductor is active only under UV light. CdS is an example of a highly active semiconductor which can be activated using visible light due to the low bandgap energy of 2.4 eV [23]. However, CdS is subject to photoanodic corrosion and this feature makes it unacceptable as a photocatalyst for water purification [24]. Among different semiconductor photocatalysts, TiO<sub>2</sub> appears as the most active and most suitable one for a wide variety of energy and environmental applications. In fact, TiO<sub>2</sub> has a high oxidation ability since its photogenerated holes is at  $E^0 = 2.9 \text{ V vs. NHE at pH } 0$ . Moreover, TiO<sub>2</sub> is biologically and chemically inert, photostable and relatively cheap [19, 25]. TiO<sub>2</sub> was used intensively in industrial products in order to replace the older toxic

lead oxides as a pigment for white paint. Recently, the world production of  $\text{TiO}_2$  passed 4 million tons every year with China as the world's largest production country [26].  $\text{TiO}_2$  has been used as a pigment in various applications involving paints, plastic, rubber, ink, papers and textile, in addition to the considerable amount of the global production used in food and pharmaceuticals product [25]. There are two commercial ways of manufacturing  $\text{TiO}_2$  namely pyrogenic and precipitation processes [25].

The pyrogenic process was improved in 1920. However, this process was not commercially applicable until the late 1950s. In this process,  $\text{TiO}_2$  was reacted with gaseous chloride in the presence of coke to produce liquid titanium tetrachloride. The product was distilled and oxidized in the vapor phase to obtain  $\text{TiO}_2$ . The precipitation process involves direct reaction between  $\text{TiO}_2$  ore and sulfuric acid, the product was then hydrolyzed to produce a hydrate oxide, which was followed by calcinations process at  $900^\circ\text{C}$  to produce  $\text{TiO}_2$  [25]. Figures 1.7(a) and 1.7 (b) show the production of  $\text{TiO}_2$  using pyrogenic and precipitate processes respectively. The type of crystalline form of  $\text{TiO}_2$  is the most important part in the determination of good photocatalyst.

There are three types crystalline forms of  $\text{TiO}_2$  namely anatase, rutile and brookite [27, 28]. Brookite is a natural phase, which is quite difficult to synthesize in a laboratory. It is also rare in nature and structurally more complex than the other two polymorphs (anatase and rutile). The rutile and anatase phases are the most used in photocatalytic studies (Figure 1.8).

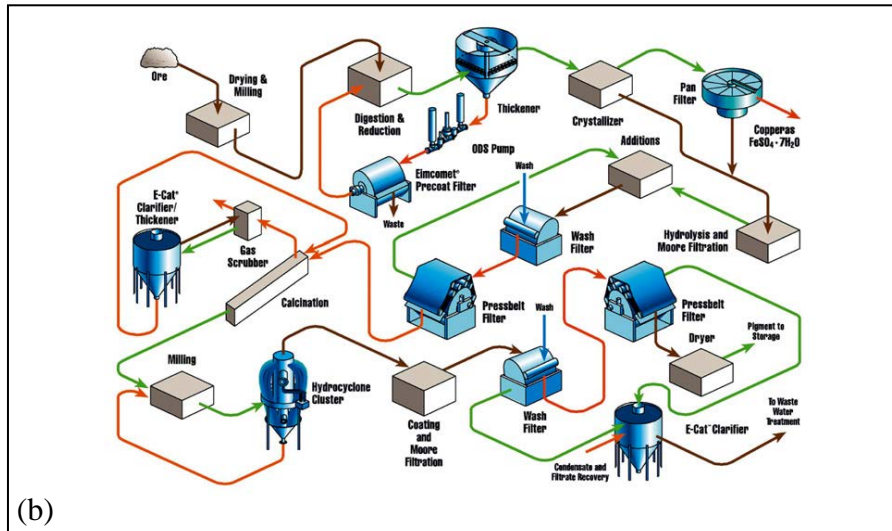
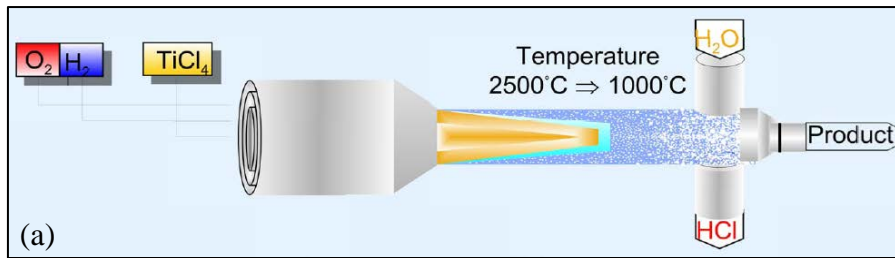


Figure 1.7: The manufacturing of  $\text{TiO}_2$  using: a) pyrogenic process, b) precipitation process [25].

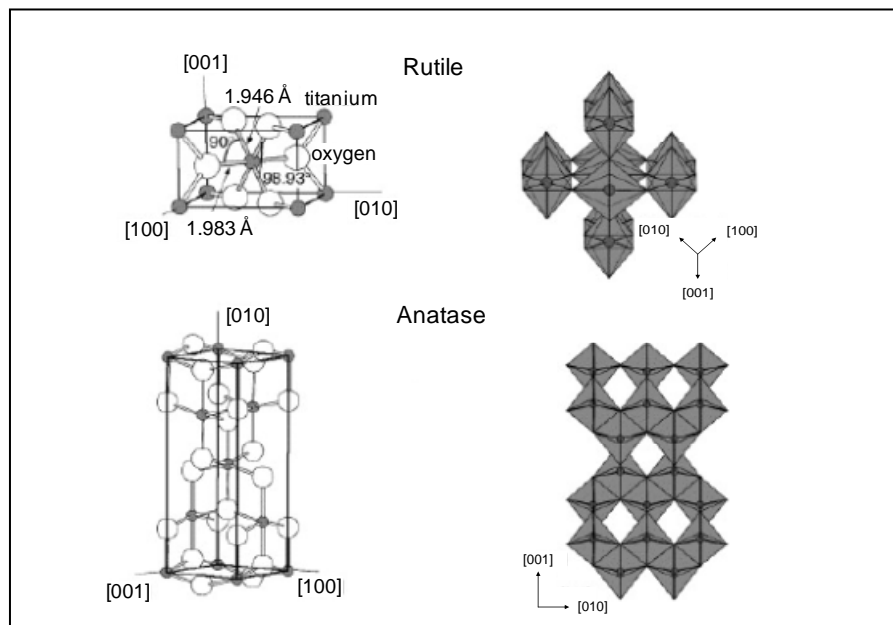


Figure 1.8: Bulk crystal structure of rutile and anatase in  $\text{TiO}_2$  [28].

Both anatase and rutile are semiconductors with the bandgap located at about 3.2 eV and 3.0 eV, respectively. Rutile does adsorb some visible light while anatase only absorbs in the UV region of spectra. Unfortunately, rutile is not a good photocatalyst [28]. Many researchers have concluded that rutile is catalytically inactive or a much less active form of TiO<sub>2</sub> [29, 30]. Rutile form of TiO<sub>2</sub> however suffers from strong recombination of electrons and holes due to the lack of defects within its crystal lattice. Anatase form of titanium dioxide therefore appears to be the most efficient semiconductor for environment application. Its photocatalytic activity is higher than most available crystalline forms of TiO<sub>2</sub>.

Rutile is the most common crystalline form of TiO<sub>2</sub> in nature. The rutile structure is not compact. Its unit cell is tetragonal where one axis is 30% shorter than the other two axes ( $a = 4.593 \text{ \AA}$ ,  $c = 2.959 \text{ \AA}$ ) [27,28,29]. The structure is constituted by distorted octahedral TiO<sub>6</sub>, with oxygen atoms shared with other adjacent Ti atoms. Every Ti atom is an octahedron surrounded by six O atoms, and every O atom is surrounded by 3 Ti atoms at the edges of an equilateral triangle. It can be envisaged as a central body cubic lattice of Ti atom that is considerably distorted. The crystallites can be present in nature as black or reddish mineral and also transparent when it comes completely without impurities. The color can also be orange if the mineral is in a very thin needle form [28].

Anatase form has tetragonal bipyramidal symmetry, with a structure similar to an elongated octahedron ( $a = 3.785 \text{ \AA}$ ,  $c = 9.514 \text{ \AA}$ ). The structure is based on a polyhedral chain of TiO<sub>6</sub>. The difference with rutile is that anatase presents a more distorted structure, where every polyhedron shares 4 edges with the adjacent one. In particular, the tetragonal elementary cell contains 4 units, instead of 2, and the cell sides are  $a = 3.785 \text{ \AA}$  and  $c = 9.514 \text{ \AA}$ . The anatase crystals are really small and the

color ranges from blue sapphire to yellow-brown [29]. These differences in lattice structures cause different mass densities and electronic band structures for the two main TiO<sub>2</sub> polymorphs. The band gap energy for anatase and rutile is equal to 3.2 and 3.1 eV, respectively. The valence band are mostly O 2p atomic orbitals-derived, while the conduction band is mostly Ti 3d-derived (Figure 1.9) [25,28]. Moreover, TiO<sub>2</sub> like other oxides is thermodynamically stable as a non-stoichiometric compound, with anion deficiencies. Therefore, a more correct denotation would be TiO<sub>2-x</sub>. Generally the material defects, such as vacancies, can introduce localized ionized states. In the case of TiO<sub>2</sub>, oxygen vacancies are formally compensated by the adoption of the +3 oxidation state by an equivalent number of titanium atoms. These Ti<sup>3+</sup> ions operate as electron donors, introducing localized levels next to the conduction band. This is due to the *n-type* semiconductor character of TiO<sub>2</sub> [25, 30].

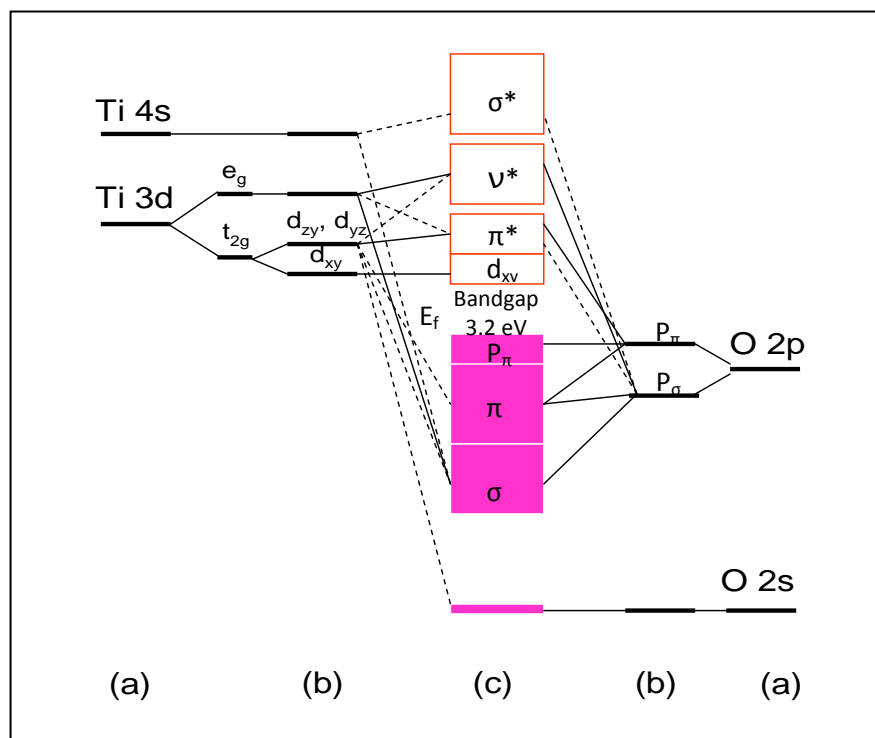


Figure 1.9: Molecular orbital structure of anatase: a) atomic levels, b) crystal – field split levels, c) final interaction states [30].

## 1.6 Mechanism of TiO<sub>2</sub> in photocatalytic reaction

Although the overall reactions of the photocatalytic semiconductor are oxidation and reduction, the main steps that cause both oxidation and reduction are still not well understood. The photocatalytic processes are divided into four phase systems namely electronic, solid, liquid and gas phases [31]. Electronic phase is the UV light source which relates to the excitation of the electron in the valence band into the conduction band. The liquid phase is the wastewater, solid phase is the catalyst and gas phase is the oxygen that contained in water. Some of the explanation about photocatalytic process of the semiconductor has been discussed in the previous section (Section 1.4). This section will provide a more detailed discussion about the mechanism involved in TiO<sub>2</sub> semiconductor photocatalyst. Figure 1.10 shows the overall mechanism of the production process of radicals from TiO<sub>2</sub>. The process of photocatalytic reaction by TiO<sub>2</sub> takes place by the absorption of ultraviolet (UV) or near-ultraviolet photons ( $h\nu$ ) that equal or exceed the band gap energy ( $E_{bg}$ ) values for anatase and rutile ( 3.2 eV and 3.1 eV ) respectively onto its surface [25,32].

An electron would separate out by photoexcitation from the valence band to the empty conduction band of the TiO<sub>2</sub> and positive hole would be left in the valence band. The mechanism of electron-hole charge separation is provided in equation 1.13. Since the catalyst is always in contact with the liquid solution, transferring of the charge would occur until it has achieved an electrostatic equilibrium [33]. In metal, excessive charge is confined on the surface. However, in a semiconductor, the excessive charge would be distributed in a region, which is called space-charge region. The existence of this region is due to the expanding region from the surface to bulk of the semiconductor. This region plays a very important role in the photocatalytic process. Due to the presence of the surface charge region, the photo-

excited electron can be separated from the hole and migrates to the particle surface. This would produce the potential gradient of electron and hole between the bulk solid and its external surface [25,31-34]. Equations 1.14 and 1.15 represent the electron-hole pairs migration.

Basically, two possibilities could occur after electron hole charge separation. The first one is the recombination of the photo-excited electron with holes and the input energy is released in the form of PL photon ( $h\nu_{\text{PL}}$ ) and heat as can be seen in Figure 1.10 and equation 1.16. Another one is that the separated electron and hole will react separately with either an electron acceptor or an electron donor (from  $\text{O}_2$  and  $\text{H}_2\text{O}$  respectively), which accumulate on the particle surface. Consequently, they initiate the reduction and oxidation processes. The  $\text{O}_2$  molecules scavenge the electron from the surface of  $\text{TiO}_2$  forming superoxide radical ( $\text{O}_2^{\bullet-}$ ). This superoxide radical then reacts with proton, eventually forming hydroperoxide radical ( $\text{HO}_2^{\bullet}$ , see equations 1.17 and 1.18). While, the reaction of trapped holes in aqueous solution ( $\text{H}_2\text{O}$ ) eventually produced hydroxyl radical ( $\text{OH}^{\bullet}$ ) as can be seen in equation 1.19 [19, 25].

Eventually, the degradation process of the pollutant occurred by the reduction-oxidation (redox) process with  $\text{O}_2^{\bullet-}$ ,  $\text{HO}_2^{\bullet}$  and  $\text{OH}^{\bullet}$  radicals into the polluted species (P) and hydroxyl radicals as illustrated in Figure 1.10. However, these entire occurrences in photocatalysis reaction depended totally on the presence of both dissolved oxygen and water molecule. In fact, without the presence of water molecule, the highly reactive hydroxyl radicals ( $\text{OH}^{\bullet}$ ) could not be generated and impeded the photocatalytic reaction of the aqueous organic pollutants [21].

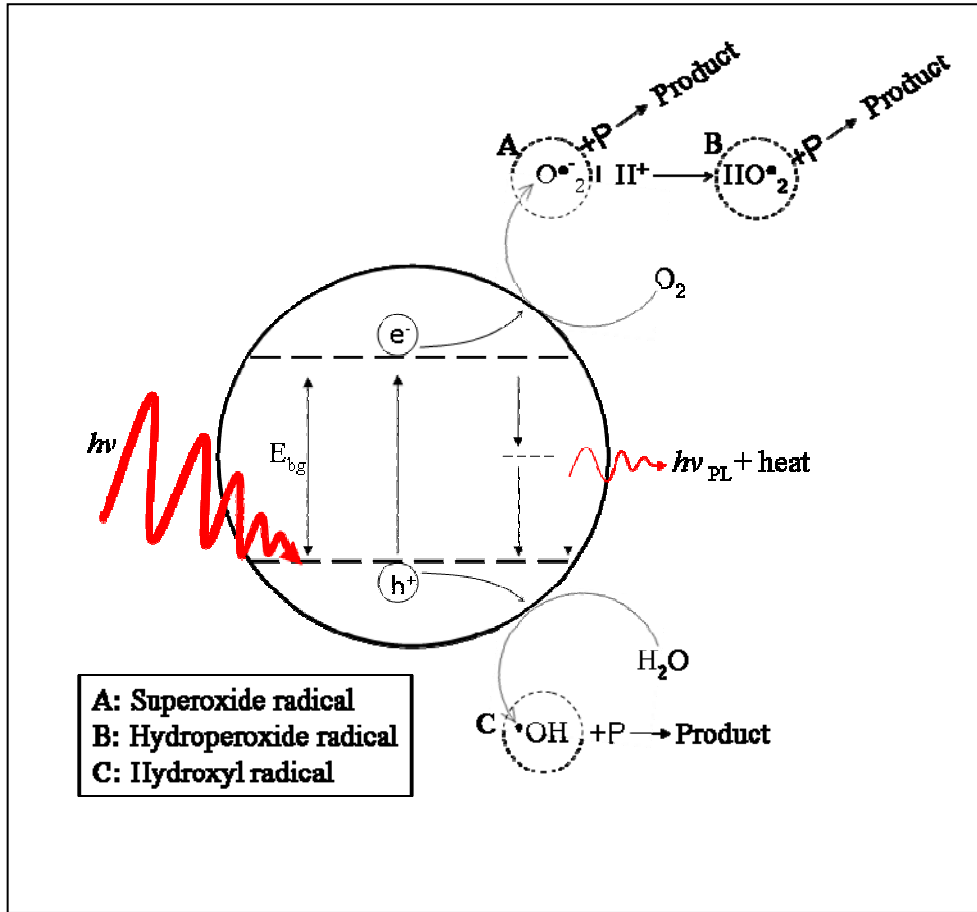
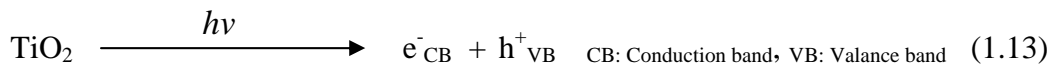
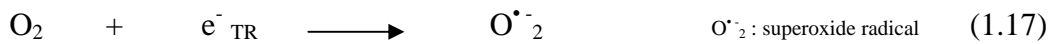


Figure 1.10: The overall mechanism involved in  $\text{TiO}_2$  photocatalyst [25].



In other words, the fundamental task of the heterogeneous photocatalyst is to generate the free radicals of the solution, mainly the highly reactive hydroxyl radical, which traditionally, is responsible for oxidizing almost all organic pollutants to CO<sub>2</sub> and H<sub>2</sub>O. Thus, during the heterogeneous photocatalytic reactions, the dissolved organic pollutants are degraded to their corresponding intermediates and subsequently mineralized to CO<sub>2</sub> and H<sub>2</sub>O [31-33]. The overall photocatalysis reaction can be depicted by equation 1.20.

Generally, in TiO<sub>2</sub> semiconductor, the incidence of recombination between electrons and holes is high which unfortunately reduces the efficiency of the photocatalytic process. The next point of view is to see the modification of TiO<sub>2</sub> to enhance its photocatalytic activity.



## 1.7 Improving TiO<sub>2</sub> photocatalytic activity

As stated earlier, one of the most active fields of research in heterogeneous photocatalysis using semiconductor particles is the development of a system capable of using natural sunlight to degrade a large number of organic and inorganic

contaminants in wastewater. The overall photocatalytic activity of a particular semiconductor system for the stated purpose is measured by several factors including the stability of the semiconductor under illumination, the efficiency of the photocatalytic process, the selectivity of the products, and the wavelength range response. TiO<sub>2</sub> is a quite stable photocatalyst, however the band gap is large ( $E_{bg} = 3.2$  eV) [31-34] making it only active in the ultraviolet region which is only 5% of the overall solar intensity [13, 14]. The limitations of TiO<sub>2</sub> as a photocatalyst for a particular use can be overcome by modifying the surface of the semiconductor to become active under visible light irradiation.

Nowadays, three benefits of modifications of photocatalytic semiconductor systems have been identified: (1) inhibiting recombination by increasing the charge separation and therefore the efficiency of the photocatalytic process; (2) increasing the wavelength response range (i.e. excitation of wide band gap semiconductors by visible light) and (3) changing the selectivity or yield of a particular product [19, 25]. A few examples will be given in the following sections illustrating the large body of work conducted in the area of photocatalyst surface modification.

### **1.7.1 Modification with metal**

The modification of TiO<sub>2</sub> by noble metal enhanced the photocatalytic process by changing the semiconductor surface properties. The metal can enhance the yield of a particular product or the rate of the photocatalytic reaction. The enhancement in reactivity was first observed using the Pt/TiO<sub>2</sub> system. The addition of Pt to the TiO<sub>2</sub> surface is beneficial for photocatalytic reactions evolving gas, especially hydrogen [35-37]. The metal actually modifies the photocatalytic properties of the semiconductor by changing the distribution of electrons. The electronic modification

of TiO<sub>2</sub> via metal deposition can also be observed with other noble metals such as Au and Ag [38-40]. Beside photocatalytic enhancement, the modification through noble metals enables TiO<sub>2</sub> particles to be active in the energy range of visible light. However, the extensive utilization of noble metals for TiO<sub>2</sub> modification as a practical remediation technology is limited because the noble metals are expensive.

For an alternative way, the modification of TiO<sub>2</sub> with transition metals provides a successful and cost effective method as compared to the costly modification with noble metals. The modification of TiO<sub>2</sub> with transition metal enhances the photocatalytic activity of the photocatalyst by UV irradiation and exceeds its application in the visible light region. It was reported that the doping of a series of transition metals in TiO<sub>2</sub> such as V, Cr, Mn, Ni and Fe brings about a red shift in the absorption pattern of the TiO<sub>2</sub> semiconducting catalyst [41,42]. The order of the effectiveness in the red shift was found to be V > Cr > Mn > Fe > Ni [43]. The transition metal modified photocatalysts exhibited absorption in the range of 400-600 nm and thus could be effectively utilized under solar and visible light irradiation. Moreover, doping of TiO<sub>2</sub> with Fe<sup>3+</sup> was affirmed to introduce much more oxygen vacancies in surface of TiO<sub>2</sub> [44]. High concentration of the Fe<sup>3+</sup> dopant however increased the recombination rate and accordingly reduced the efficiency of the photocatalytic activity [45].

### **1.7.2 Modification with nonmetals**

Modification of TiO<sub>2</sub> with nonmetals is an advance modification process in the development of visible light responsive TiO<sub>2</sub> photocatalyst. Nitrogen (N), carbon (C) and sulphur (S) are the most popular elements being studied by researchers and may have a bright potential for commercialization.

### 1.7.2.1 Nitrogen doped TiO<sub>2</sub>

The modification of TiO<sub>2</sub> using nitrogen was first discovered by Asahi et al. [46,47]. They proposed that N atoms became incorporated into the lattice of TiO<sub>2</sub> by substituting the site of oxygen atoms. The corresponding N (2p) states results in a reduction of the band gap of the N-doped TiO<sub>2</sub> thus increasing the possibility for the modified photocatalysts to be utilized under visible light irradiation [48].

In general, the N-doped TiO<sub>2</sub> has been successfully prepared either by a reduction process using gaseous NH<sub>3</sub> [49,50], oxidation of TiN [50,51], treating of TiO<sub>2</sub> and urea mixtures [50,52-54], sputtering of the TiO<sub>2</sub> target in N<sub>2</sub> atmosphere [50,55], or hydrolysis or hydrothermal treatment of a titanium containing precursor with NH<sub>3</sub> solution [56]. The improvement of visible light photocatalytic activity of nitrogen doped TiO<sub>2</sub> was usually attributed to the decrease of the band gap through hybridization of the N 2p states with O 2p states on the top of the valence band or the creation of a N-induced mid-gap level just above the O 2p valence band maximum (VBM) [49-56]. However, recent electronic structure calculation indicated that there was virtually no shift of the upper edge of the O 2p valence band for the nitrogen doped TiO<sub>2</sub>. Instead, occupied N 2p localized states appeared slightly above the valence band edge [57].

The current interesting focus in the field of N-doped TiO<sub>2</sub> is to clarify the N states in TiO<sub>2</sub> which are usually investigated by X-ray photoelectron spectroscopy (XPS). However, the assignment of N 1s peaks is still in controversy in the literatures [58]. In general, the peak of N 1s in the XPS spectra mostly lies in the range of 396–404 eV [51,56,58,59]. Most reports agreed that N 1s peak at 396–398 eV was the characteristic peak of Ti–N linkages, indicating that nitrogen atom is doped into the TiO<sub>2</sub> lattice and is responsible for the enhanced activity [51,56,59].